International Journal of Biological Macromolecules 192 (2021) 90–99

Contents lists available at ScienceDirect

International Journal of Biological Macromolecules

journal homepage: www.elsevier.com/locate/ijbiomac

Conformational flexibility of the conserved hydrophobic pocket of HIV-1 gp41. Implications for the discovery of small-molecule fusion inhibitors

Mario Cano-Muñoz *, Samuel Jurado [1], Bertrand Morel [2], Francisco Conejero-Lara *

Departamento de Química Física, Instituto de Biotecnología y Unidad de Excelencia de Química Aplicada a Biomedicina y Medioambiente (UEQ), Facultad de Ciencias, Universidad de Granada, 18071 Granada, Spain

ARTICLE INFO

Keywords:
Binding cooperativity
Coiled-coil
Allosterism
Calorimetry
Antiviral therapy

ABSTRACT

During HIV-1 infection, the envelope glycoprotein subunit gp41 folds into a six-helix bundle structure (6HB) formed by the interaction between its N-terminal (NHR) and C-terminal (CHR) heptad-repeats, promoting viral and cell membranes fusion. A highly preserved, hydrophobic pocket (HP) on the NHR surface is crucial in 6HB formation and, therefore, HP-binding compounds constitute promising therapeutics against HIV-1. Here, we investigated the conformational and dynamic properties of the HP using a rationally designed single-chain protein (named covNHR) that mimics the gp41 NHR structure. We found that the fluorescent dye 8-anilino-naphtalene-1-sulfonic acid (ANS) binds specifically to the HP, suggesting that ANS derivatives may constitute lead compounds to inhibit 6HB formation. ANS shows different binding modes to the HP, depending on the occupancy of other NHR pockets. Moreover, in presence of a CHR peptide bound to the N-terminal pockets in gp41, two ANS molecules can occupy the HP showing cooperative behavior. This binding mode was assessed using molecular docking and molecular dynamics simulations. The results show that the HP is conformationally flexible and connected allosterically to other NHR regions, which strongly influence the binding of potential ligands. These findings could guide the development of small-molecule HIV-1 inhibitors targeting the HP.

1. Introduction

Enveloped viruses with class-I fusion type machines, such as the Human Immunodeficiency Virus (HIV), Ebola Virus (EboV), Human Respiratory Syncytial Virus (HRSV), Influenza virus, and coronaviruses like Severe Acute Respiratory Syndrome Coronavirus (SARS-CoV) or the recently emerged SARS-CoV-2, currently constitute an undoubtedly major threat to humanity (public health and economic issue) [1–3]. Although the major focus is currently set on the dramatic Coronavirus Disease 2019 (COVID-19) pandemic, we cannot forget that the HIV pandemic is still very active and continues to be one of the world's largest pandemics with near than 1 million deaths annually [4].

Regarding HIV, the causative agent of Acquired Immune Deficiency Syndrome (AIDS), modern Highly Active Antiretroviral Therapies (HAART) have been developed and have helped reducing the mortality and morbidity associated with the infection. Nevertheless, the emergence of multi-resistant HIV variants to the current treatment and the appearance of side effects and drug-drug interactions promote the necessity of continuing to discover and produce new inhibitors directed towards different stages in the virus' life cycle [5,6].

The entry of virion particles into the host cell by fusing both membranes is a key step in the infection of HIV, thus, it has long been considered as an attractive target for the development of new anti-HIV drugs [1]. Conceivably, inhibition of the fusion process prevents the infection by an active viral particle and thus, investigation in this respect may yield compounds that can potentially serve as prophylactics and antivirals.

The fusion process is mediated by the envelope glycoprotein (Env), a non-covalently associated trimer of heterodimers composed of two glycoprotein subunits, gp120 and gp41 [7]. The binding of HIV-1 gp120 to CD4 receptor and a co-receptor, CCR5 or CXCR4, on surface of the target cell, initiates the fusion process. This event in gp41 triggers a

Abbreviations: ANS, 8-anilino-naphtalene-1-sulfonic acid; DSC, differential scanning calorimetry; ITC, isothermal titration calorimetry; CD, circular dichroism; DLS, dynamic light scattering; SLS, static light scattering; NHR, N-terminal heptad repeat; CHR, C-terminal heptad repeat; HP, gp41 hydrophobic pocket.

* Corresponding authors.
E-mail addresses: mariocano@ugr.es (M. Cano-Muñoz), conejero@ugr.es (F. Conejero-Lara).
[1] Present address: Diater Laboratorio farmacéutico, Av. Peces Barba n° 2, Parque tecnológico Leganés, 28918, Spain.
[2] Present address: Angany Innovation, 1 voie de l'innovation, Pharmaparc II, 27100 Val de Reuil, France.

https://doi.org/10.1016/j.ijbiomac.2021.09.198
Received 3 August 2021; Received in revised form 24 September 2021; Accepted 29 September 2021
Available online 5 October 2021

series of large conformational changes, in which three N-terminal heptad repeat (NHR) regions form an inner helical coiled-coil core trimer and three C-terminal heptad repeat (CHR) regions associate externally with the NHRs in an antiparallel fashion, ultimately adopting a six-helix bundle conformation (6HB) [8,9]. This energetically favorable interaction between NHR and CHR brings viral and host-cell membranes into close proximity promoting fusion and eventually causing infection. Consequently, compounds that interact with either CHR or NHR may interfere with this key process and thereby constitute HIV fusion inhibitors [10].

Traditionally, peptides with sequence derived from those regions have been developed as promising inhibitors. However, the CHR-derived peptide T20 is still the only FDA approved fusion inhibitor [11]. This is in part due to the drawbacks associated with the use of peptide-based compounds, such as its lack of oral bioavailability and short half-life in vivo due to rapid proteolytic cleavage and renal filtration, which forces it to be administered by subcutaneous injection twice daily in very high dosage. These problems, together with its high cost of production, make T20 only used as salvage therapy [12]. Therefore, the identification of new small-molecule compounds targeting gp41 with high oral bioavailability and lower production costs is urgently needed.

On this basis, small-molecule compounds still constitute promising therapeutics agents. This search for highly active compounds could be made either by optimizing existent inhibitors or by finding new pharmacophore structures not evaluated before, or even following both strategies, i.e., finding new structures to further optimize them.

In the gp41 6HB structure, a deep hydrophobic pocket (HP) on the NHR surface has proven to be of high importance in the NHR-CHR interaction [9] and its occupancy interferes with 6HB formation and thereby with membrane fusion [13]. Although small-molecule based strategies targeting gp41 have been widely explored in the past and a large number of small-molecule ligands have been described [10,14,15], such as NB-2 and NB-64 including its derivatives [13] or indole-based compounds [16], the compounds identified to date exhibit limited in vitro potency and their affinity towards their target is usually moderate. Many of these strategies have made use of stabilized chimeric variants of the NHR region of gp41, such as IZN17 [17] and 5-helix [18], as templates exposing the HP in order to sieve compound libraries (following both virtual and experimental approaches) [19]. Nevertheless, they have not achieved the expected success for reasons that remain not well understood. A major challenge is to find a model that can truly mimic the dynamic conformation of the HP in the prefusion intermediate of gp41. It has also been pointed out that the HP may be too big or too deep for small-molecule inhibitors to achieve a sufficiently high affinity that can compete with the internal CHR interaction, and that a potent inhibitor may need additional interactions outside the HP to acquire potent activity [15]. For these reasons, a more complete understanding of the conformational and dynamic properties of the HP and its relationships with other gp41 pockets would shed light on these issues and guide the discovery of new and more active molecules.

Recently, our group has designed, produced and characterized single-chain chimeric protein constructs (named covNHR, Fig. 1) that accurately mimic the structure of NHR in gp41 [20,21]. In contrast to gp41, which is a transmembrane protein, highly insoluble in aqueous solvents at physiological pH [22], covNHR is a very stable, highly soluble and easy-to-produce recombinantly in *E. coli* strains. The solved crystallographic structure of covNHR in complex with the CHR-derived peptide C34 (PDB ID: 6R2G) shows a virtually identical binding interface to that present in other gp41 constructs in post-fusion conformation [21]. Thus, it constitutes an interesting target to be employed as a template for the search of small-molecule compounds directed against gp41.

8-Anilinonaphtalene-1-sulfonic acid (ANS) is a well-known fluorescent probe that binds to solvent-exposed hydrophobic patches in proteins and is widely used to characterize exposed hydrophobicity and

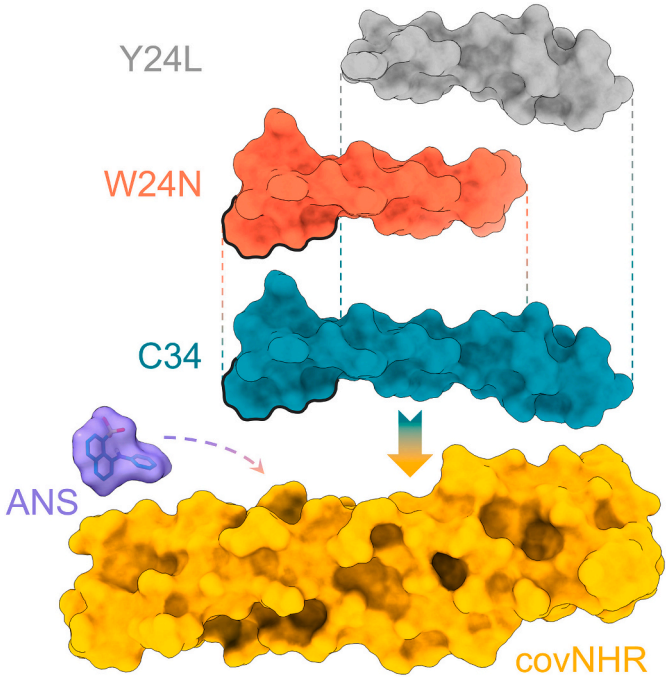

Fig. 1. Overall layout of the molecules involved in this study. The structure of the protein and peptides involved is taken from the crystal structure of the complex between covNHR and C34 peptide (PDB ID: 6R2G), depicted in yellow and cyan surface respectively. The structure of W24N and Y24L peptides, depicted in red and gray surfaces, is derived from that of C34 in the complex structure. The pocket-binding domain is highlighted in black lines for C34 and W24N peptides. ANS molecule is represented in sticks and in purple semi-transparent surface. CovNHR is a highly accurate mimic of the trimeric NHR coiled-coil, with the advantage of exposing only one single interface for CHR binding, see details in the text.

partial unfolding or misfolding in proteins [23]. ANS exhibits drug-like physicochemical properties [24] present in many other small-molecule gp41 inhibitors inspected to date, such as a low molecular weight (<500 Da), an amphiphilic structure and the presence of a negative charge at biological pH [12,16]. Due to these special properties, ANS could constitute an excellent probe to investigate the conformational properties and interactions at the HP.

In this study, we investigated the binding of ANS with the covNHR protein in the presence and absence of interactions with CHR-derived peptides (Fig. 1). We found that ANS can bind specifically to the HP but its binding mode is strongly modulated allosterically by other distant NHR-CHR interactions, which are relevant in the gp41-mediated fusion process. Our results confirm a previously hypothesized allosteric communication between different NHR pockets and may help in guiding the identification of new small-molecule inhibitors targeting the gp41 NHR region.

2. Materials and methods

2.1. Protein and ligands samples

The DNA encoding the covNHR protein sequences was synthesized by Thermofisher Scientific (Waltham, USA). In order to facilitate purification by Ni-Sepharose affinity chromatography, the protein sequences were histidine tagged at the C-terminus. CovNHR proteins were produced by overexpression in *E. coli*, as described previously [20]. Synthetic CHR peptides, both *N*-acetylated and C-amidated, were acquired from Genecust (Luxembourg), with a purity >95%. Protein and peptide concentrations were determined by UV absorption measurements at 280 nm with extinction coefficients calculated theoretically according to

their amino acid sequences with the ExPasy ProtParam server (https://web.expasy.org/protparam/) [25]. 8-Anilino-naphtalene-1-sulfonic acid (ANS) was purchased from Honeywell Fluka (Sigma-Aldrich, St. Louis, Missouri, United States). The concentration of ANS was quantified by UV–visible spectrophotometry using a molar extinction coefficient of 7800 $M^{-1}{\cdot}cm^{-1}$ at 370 nm [26].

2.2. Fluorescence measurements

Fluorescence spectra were measured on a Varian Cary Eclipse spectrofluorimeter (Mulgrave, Victoria, Australia) equipped with a four-cell block temperature controller using a 3 mm path length quartz cuvette. ANS binding to the protein constructs was monitored by measuring the fluorescence emission spectra between 400 and 600 nm following excitation at 370 nm at 25 °C. Slit widths were set to 5 nm for both the excitation and emission monochromators. The resulting spectra were the average of 5 individual scans.

All measurements were performed in 50 mM sodium phosphate buffer at pH 7.4 at 25 °C with a protein concentration of 10 μM and samples were equilibrated for 5 min prior to measurement. No alteration in pH of the protein or complex solutions was observed in the presence of up to 800 μM ANS. For the titration experiments with ANS the total protein and peptide (if present) concentrations were kept constant whereas the ANS concentration was varied between 0 and 250 μM. ANS titration experiments in presence of CHR-derived peptides were carried out at a fixed 1:2 molar ratio between the protein and the peptide; Peptide titrations in presence of ANS were performed at a 1:3 molar ratio (protein:ANS), unless stated otherwise. Due to the relatively high absorbance of ANS reached in the titrations, the fluorescence emission was corrected from the inner filter effect as described elsewhere [27].

2.3. Circular dichroism

Circular dichroism (CD) experiments were conducted on a Jasco J-715 spectropolarimeter (Jasco, Tokyo, Japan) equipped with Peltier-thermostatic cell holder using a bandwidth of 1 nm, a scan rate of 100 nm/min and a response time of 1 s. Near-UV CD spectra (450–250 nm) were measured at a protein concentration of ~40 μM using a 5 mm quartz cuvette and are the result of the average of 20 individual scans. The interaction experiments were carried at a 1:2 molar ratio between the protein and each CHR-derived peptide and at a 1:3 molar ratio between the protein and ANS ligand. Each spectrum was corrected by baseline subtraction using the blank spectrum obtained with the buffer and finally the CD signal was normalized to molar ellipticity ([θ], in $deg{\cdot}dmol^{-1}{\cdot}cm^{2}$).

2.4. Isothermal titration calorimetry

ITC experiments were performed in a Microcal VP-ITC calorimeter (Malvern Instruments, Worcestershire, UK). The protein solutions were typically titrated with 25–30 injections of 5 μL or 10 μL ANS solution using an interval of 480 s, the stirring rate was 300 rpm and the reference power for the baseline was set to 10 μcal/s. Concentrations of the protein used for the titrations were 10 μM to 40 μM, while ANS in the syringe was between 450 μM and 1000 μM. When the CHR-derived peptide was present it was added at a ratio of 1:2 between the protein and the peptide to reach saturation. All experiments were carried out in 50 mM phosphate buffer, pH 7.4 at 25 °C.

The experimental thermograms were baseline corrected and the peaks were integrated to determine the heats produced by each ligand injection. As a blank, an independent experiment with only buffer in the calorimeter's cell was performed with the same ANS solution to determine the corresponding heats of dilution. Finally, each heat was normalized per mole of added ligand. The resulting binding isotherms were fitted using different binding models, as described in the Results. Additional details of the binding models are provided in the Supplementary Text S1.

2.5. Dynamic and static light scattering

The apparent hydrodynamic radii of the protein and protein-ligand complexes were measured using dynamic light scattering (DLS) in a DynaPro MS-X DLS instrument (Wyatt, Santa Barbara, CA, USA). Dynamics v6 software (Wyatt Technology Corporation, Santa Barbara, CA, USA) was used in data collection and processing. Sets of DLS data were measured at 25 °C with an average number of 50 acquisitions and an acquisition time of 10 s. Measurements were carried out in 50 mM sodium phosphate buffer pH 7.4. Static scattering intensities were also measured at different concentrations of protein in a range of 0.2 to 3.5 mg mL^{-1}. The intensities were analyzed using the Debye plot as represented by Eq. (1),

$$Kc/R_{90} = 1/M_w + 2A_2c \quad (1)$$

valid for particles significantly smaller than the wavelength of the incident radiation, where K is an optical constant of the instrument, c is the particle mass concentration, R_{90} is the Rayleigh ratio of scattered to incident light intensity, M_w is the weight-averaged molar mass, and A_2 is the 2nd virial coefficient that is representative of inter-particle interaction strength. M_w can be determined from the intercept of the plot.

2.6. Molecular modeling and docking studies

The high-resolution crystal structure of covNHR in complex with the CHR-derived peptide C34, previously determined by our group, was retrieved from the Protein Data Bank (PDB ID: 6R2G) [21]. To model the structure of the free covNHR protein, we removed the C34 peptide, the water molecules and the phosphate ion present in the structure, and added missing hydrogens and heavy atoms in the coordinate file. After that, we modeled the first loop, which was undefined in the crystal structure, using the Build Loop tool of YASARA Structure (v17.12.24) [28]. The model was then subjected to energy minimization to remove bumps and correct the covalent geometry; the structure was energy-minimized with the NOVA force field [29], using an 8 Å distance cut-off and the Particle Mesh Ewald algorithm [30] to treat long-range electrostatic interactions. After removal of conformational stress by a short steepest descent minimization, the procedure continued by simulated annealing (time step 2 fs, atom velocities scaled down by 0.9 every 10th step) until convergence was reached, i.e. the energy improved by less than 0.05 kJ mol^{-1} per atom during 200 steps.

AutoDock 4.2 [31] was used to examine how ANS interacts with covNHR in both the free and peptide-bound forms. Docking was performed using the default docking parameters and point charges initially assigned according to the AMBER03 force field [32] and then the partial charges of atoms were calculated using the less polar Gasteiger-Marsili method to optimize the AutoDock scoring function. The 2D structure of the ANS ligand was drawn using the ChemDraw software, adding hydrogen atoms. The ANS structure was energy minimized by PM3 semiempirical techniques and the molecule was saved as a PDB format file prior to docking as described elsewhere [33]. A box 5 Å larger than the protein receptor in every dimension was generated with covNHR as the centroid. The Lamarckian genetic algorithm (LGA) [34] was used to search 100 independent ligand conformations and during the docking experiment the ligand was set as “flexible” meaning that it could be oriented within the grid box to generate different binding conformations while the protein was kept as “rigid”, i.e. in a fixed conformation.

At the end of the docking experiments, the structures were ranked by energy and ligand-protein interactions were all visualized on the basis of docking results. The best docking poses were selected based on the estimated binding energy of the lowest energy conformation of the highest populated cluster and the best interactions between ligand and protein. The setup, modeling, visualization and analysis were performed

with the YASARA molecular modeling program [28].

2.7. Molecular dynamics simulations

All-atom molecular dynamics simulations were performed using YASARA Structure (v.17.12.24) [28] under the same parameters with explicit solvent (TIP3P water, the solvent density was equilibrated to a final value of 0.997 g/mL) in a periodic box with size 10 Å larger than the protein in every dimension. In order to describe long-range electrostatics, Particle Mesh Ewald (PME) [30] method was used with a cutoff distance of 8 Å at physiological conditions (0.9% NaCl, pH 7.4), constant temperature (298 K) using a weakly-coupled Berendsen thermostat and constant pressure (1 bar). Ewald summation was used to assign amino acids charge according to their predicted side chain pK_a and was neutralized by adding counterions (NaCl) [35]. The AMBER14 [36] force field was used together with multiple time step integration where intra-molecular forces were calculated every 2 fs and inter-molecular forces every 2.5 fs. The structures were initially energy-minimized using first steepest descent without electrostatics to remove steric clashes and conformational stress, and subsequently relaxed by steepest descent minimization and simulated annealing (time step 2 fs, atom velocities scaled down by 0.9 every 10th step) until convergence was reached, i.e. the energy improved by less than 0.05 kJ mol^{-1} per atom during 200 steps. The minimized system was slowly heated up during an equilibration phase until the target temperature and density were reached. Every system was simulated for a minimum of 100 ns and coordinates were saved every 10 ps, yielding 10,000 time points for each trajectory.

3. Results and discussion

3.1. ANS binds specifically to the gp41 hydrophobic pocket

ANS is an amphiphilic fluorescent dye that is commonly used to assess the presence of solvent-exposed hydrophobic patches in proteins [23]. To determine whether ANS can bind to covNHR we carried out ANS fluorescence emission experiments upon excitation at 370 nm. We found out that ANS binding to covNHR produced a fluorescence emission band with a maximum intensity at ~468 nm (Fig. 2A), characteristic of ANS binding to hydrophobic surfaces in proteins. Due to the reported ability of ANS to bind nonspecifically to a variety of surfaces in proteins we wanted to verify whether this fluorescence signal accounted for specific or nonspecific binding of ANS to covNHR.

We previously demonstrated that covNHR binds with very high affinity to several CHR derived peptides (such as the well-known C34 peptide) [21,37]. C34 (gp41 residues 117–150) interacts with three NHR sub-pockets, a N-terminal polar pocket (NTP), a shallow middle pocket (MP), as well as the HP. When added to the covNHR-ANS mixture, C34 decreased strongly the ANS fluorescence emission to a residual value (Fig. 2A), implying that this HP binding peptide can displace ANS from its binding location. A shorter peptide, W24N (residues 117–140), which also binds to the HP and the MP but does not cover the NTP, produced an identical fluorescence emission decrease.

In contrast, the Y24L peptide, which also binds to covNHR with high affinity (~90 nM) covering the NTP and the MP but lacking the HP binding motif, produced a lower decrease in ANS fluorescence emission, although the maximum ANS fluorescence intensity was red-shifted by ~9–10 nm. This bathochromic shift indicates a change to a more polar environment of bound ANS in presence of this peptide, suggesting a change in the binding mode of ANS to the HP.

To delimitate more precisely the location of the ANS binding site, we tested ANS binding against two covNHR miniproteins, each mimicking the N-terminal and C-terminal halves of the NHR region in gp41 (covNHR-N and covNHR-C respectively) [38]. CovNHR-N displays in its surface the NTP and MP sub-pockets, while covNHR-C exposes the HP and a minor C-terminal pocket (CTP). As expected, ANS fluorescence

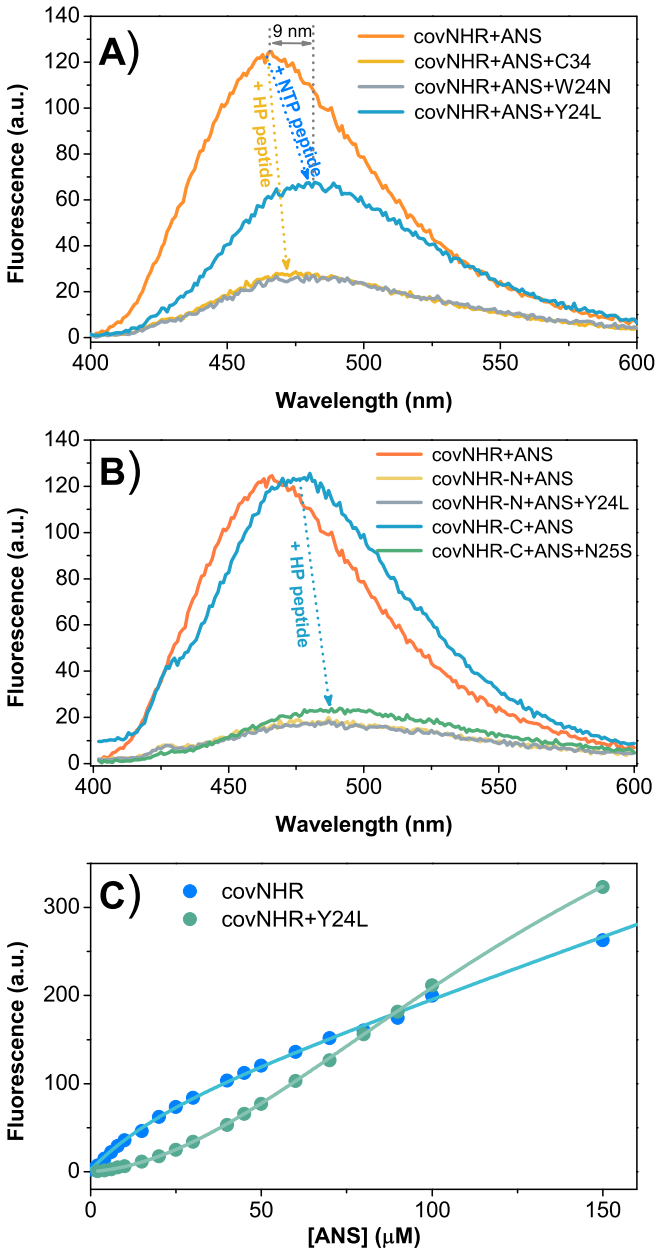

Fig. 2. Binding of ANS monitored by fluorescence. A) ANS fluorescence spectra in its 3:1 mixture with 10 μM covNHR in its free form and in presence of different CHR peptides (2:1 peptide to protein ratio). W24N and C34 peptides bind to the HP, whereas Y24L does not. B) Fluorescence spectra of ANS mixed at 3:1 ratio with shortened versions of covNHR [38], displaying different pockets of the NHR crevice. CovNHR-N displays the NTP and MP, whereas covNHR-C displays the HP and CTP. Addition of the N25S peptide abolishes the interaction of ANS with the HP pocket of covNHR-C. C) Fluorescence titration experiments of covNHR and ANS in presence (green) and absence (blue) of Y24L peptide showing the effect that this peptide causes in the mode of binding of ANS.

was only marginal in its mixture with covNHR-N and did not change in presence of bound Y24L peptide (Fig. 2B). However, ANS bound to covNHR-C induced a similar fluorescence emission band to that found upon ANS binding to covNHR. Interestingly, in presence of the N25S peptide, complementary to covNHR-C, the ANS fluorescence emission decreased to the residual intensity. This confirms that only peptides harboring the HP binding motif are able to efficiently reduce ANS fluorescence emission and evidences that the HP is the actual site for specific binding of ANS.

It is interesting to see how the maximum in the emission spectra of ANS in complex with covNHR-C is also red-shifted (~9 nm from 468 to 477 nm) compared to ANS bound to covNHR. This red-shift effect, frequently associated to a change in polarity of the environment of the fluorophore, also emerges when ANS binds to the covNHR-Y24L complex, suggesting a similar change in the ANS bound conformation.

To further investigate the binding of ANS to the HP, we carried out a direct titration of covNHR with ANS measuring fluorescence emission using a protein concentration of 10 μM (Fig. 2C). The titration shows an initial parabolic dependence of fluorescence intensity with ANS concentration, corresponding to a singular binding event, followed by a linear dependence that could be attributed to unspecific binding. Intensity does not reach a plateau within the concentration range explored. Preliminary fitting of the titration curve using a simple model of 1:1 binding followed by a linear fluorescence increase complies with relatively low apparent binding affinity (K_d ~13 μM).

Next, we studied the titration of 10 μM covNHR with ANS in presence of 2:1 molar ratio of the Y24L peptide, sufficient to saturate the protein with the peptide. The fluorescence titration curve (Fig. 2C green) does not comply with a simple binding event and there seems to be a sort of cooperative behavior in ANS binding at low concentrations giving rise to a sigmoidal shape. Saturation of the fluorescence intensity at high ANS concentration is not reached in this experiment.

3.2. Dual binding mode of ANS

Circular dichroism (CD) in the near-ultraviolet (near-UV) wavelength region can provide information on the local asymmetric environment of aromatic groups in proteins due to interactions established within the tertiary structure and is sensitive to the relative orientation and proximity of other aromatic groups [39], such as those present in ligands like ANS. Previously, we have shown that the free covNHR protein presents a weak negative band at ~280 nm, corresponding to the Trp143 sidechain (Trp60 in gp41 sequence) present in the HP, but in complex with CHR peptides stacking of two CHR tryptophan side chains (gp41 residues Trp117 and Trp120) into the HP causes the appearance of a characteristic negative ellipticity band centered at 293 nm [20,21,37].

Here, we have found that binding of ANS to covNHR also produces a specific sharp negative ellipticity band at 281 nm (Fig. 3), comparable in intensity to that caused by the interaction of CHR peptides with the HP. This band may have contributions from the aniline moiety of ANS and the Trp sidechain at the HP. In addition, a weaker and broader positive band at ~340 nm is also developed, attributable to immobilization of the naphthalene moiety [40]. The CD bands, therefore, seem to be induced by the ANS aromatic groups interacting with Trp60, consistently with the idea of ANS specific binding to the HP. These specific CD bands produced upon ANS binding to covNHR are completely abolished by the addition of C34 or W24N in 1:2 molar ratio, which instead elicit the appearance of the characteristic band at 293 nm, meaning that the pocket binding motif of the CHR peptides fully displaces ANS from the HP.

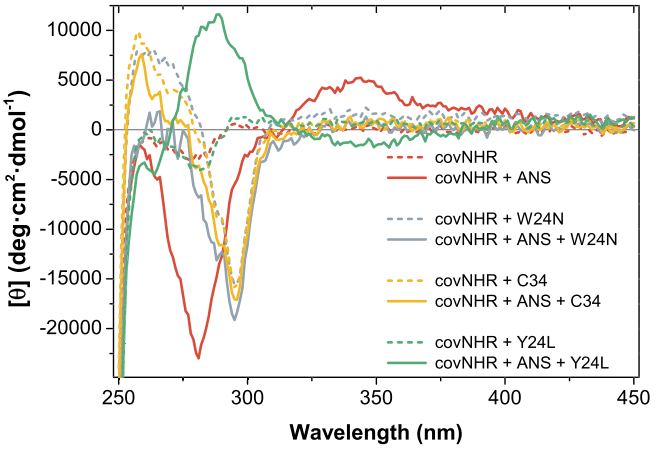

Fig. 3. Effect of ANS binding on circular dichroism spectra. Near-UV CD spectra of ANS mixtures (3:1 molar ratio) with free covNHR protein and in presence of CHR peptides (2:1 molar ratio). The protein concentration was 40 μM. Spectra in absence of ANS (light red, light yellow and light gray) were taken from reference [37].

Remarkably, when ANS binds to covNHR in presence of Y24L peptide, devoid of the HP binding motif, a positive CD band appears centered at around ~285 nm and a negative band at ~343 nm, approximately mirroring the CD spectrum of ANS bound to free covNHR and suggesting a change in the spatial orientation of bound ANS. This finding is in agreement with the hypothesis that the presence of Y24L bound to covNHR alters ANS mode of binding to the HP. This implies an allosteric communication between the different binding pockets along the NHR crevice, as previously proposed [37].

3.3. Thermodynamics and stoichiometry of ANS binding

We used ITC to investigate the interaction between ANS and covNHR, both in its free form and in presence of Y24L peptide. First, we carried out a direct ANS titration of free covNHR at 10 μM and 36 μM (Fig. 4A). The negative peaks obtained in the ITC thermogram indicate an exothermic interaction. In addition, at low protein concentration the normalized heats were very small but increase strongly at high protein concentration. The shape of the binding isotherms is not sigmoidal but hyperbolic, and the heats do not tend to zero at high ANS to protein ratios.

Preliminary analysis of the ITC isotherm at high concentration using a binding model of n-independent and identical sites does not allow a good fitting. Fixing the binding stoichiometry to values lower than 1:1 produces a reasonable description of the ITC isotherm (Fig. S1), suggesting that ANS may be binding to more than one covNHR molecule or even favoring its self-association. This would explain the observed concentration dependence of the ITC isotherms.

We recently reported the characterization of several covNHR

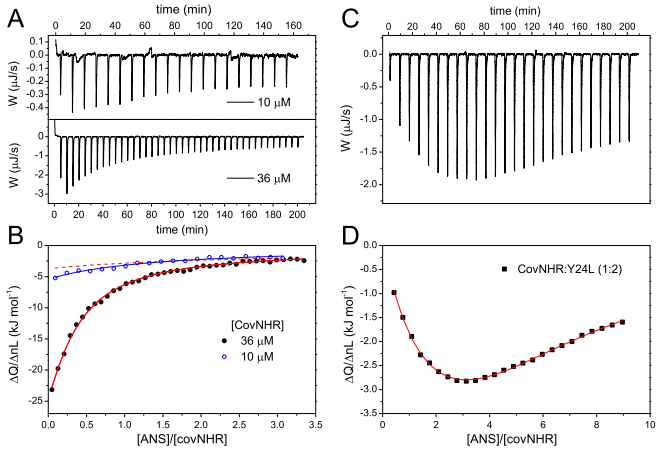

Fig. 4. ITC analysis of the interaction between ANS and covNHR in presence and absence of bound Y24L peptide. A) ITC thermograms for the ANS titration of covNHR at 10 μM and 36 μM; B) binding isotherms analyzed with a model of binding coupled to dimer formation (2 M + A ↔ M_2A). Dashed red line represents the simulated isotherm for the titration at 10 μM using the parameters of the titration at 36 μM. C) ITC thermograms for the ANS titration of covNHR at 35 μM in presence of 70 μM Y24L peptide; D) binding isotherm analyzed with a two-site sequential binding model. Symbols represent the experimental heats per mole of added ANS. The solid line corresponds to the best fits with the model.

mutants, in which buried polar residues at core positions in the coiled-coil where replaced by isoleucine [41]. These mutants show a significantly higher propensity to self-associate as dimers compared to the reference covNHR protein, which is mainly monomeric at low concentrations although it also maintains a residual propensity to dimerize at high concentrations (above ~75 μM). To test the possibility that ANS binds preferentially to covNHR dimers, we fitted the ITC isotherm using a model of ligand binding coupled to dimer formation ($2M + A \leftrightarrow M_2A$; see Supplementary Text S1 for details of this analysis). The model fits satisfactorily the ITC data supporting a binding stoichiometry of two covNHR proteins to one ANS molecule (Fig. 4B). To explain the protein concentration dependence of the binding isotherm, we simulated the binding curve of the ITC titration at 10 μM using the fitting parameters obtained with the titration at 36 μM. Although the correspondence is not perfect, the curve is very close and can be perfectly adjusted with quite similar parameters.

To support this binding mode, we carried out a similar ANS titration of the mutant protein covNHR-Q23I, which contains three core Q-I mutations that promote a higher dimerization propensity [41]. The ITC data could also be very well fitted with the model of binding to the dimer (Fig. S2). The thermodynamic parameters obtained from these analyses (Table 1) indicate a strongly exothermic binding for both protein variants, which suggests a considerable stabilization of the proteins induced by the coupled processes of ANS binding and dimerization.

To further confirm the anomalous binding stoichiometry of ANS, we carried out dynamic and static scattering measurements to elucidate the influence of ANS upon the molecular size of the protein. DLS measurements (Table S1) show an increment in the apparent hydrodynamic radii (R_h = 3.1 nm) of the covNHR protein in presence of ANS in 2:1 molar ratio, compared to that of the free protein (2.7 nm), which exhibits a value expected for a monomer, indicating an event of self-association favored by ANS. This effect is reverted in the complex covNHR:Y24L (2.8 nm) and in the complex covNHR:Y24L:ANS (2.7 nm) indicating that peptide binding shifts the equilibrium towards the monomeric state even in presence of ANS.

Static light scattering measurements confirmed that ANS binding favors the dimerization of covNHR, compared to the free protein (Fig. 5), since the Debye plot intercepts provide absolute values of the molecular weights. Only at very low concentrations, the binding of ANS to the monomeric protein could perhaps be relevant but the low sensitivity of the ITC data at these low protein concentrations do not allow an accurate determination of the binding parameters to the monomer. The binding mode of ANS to the covNHR dimer may imply the mutual insertion of the Trp143 side chains of each covNHR protomer into the reciprocal HP and aromatic stacking with the ANS groups. We observed a similar interaction in the crystal structure of the free covNHR molecule (PDB code: 4R61) [20].

In sharp contrast, the covNHR:Y24L complex showed a monomeric state in all the concentration range studied, as demonstrated in the Debye plot of Fig. 5. Moreover, ANS binding to this complex does not appear to induce any dimerization. These results further support a mechanism of ANS-mediated dimerization of the free protein as proposed above. In addition, occupancy of the NHR crevice by the Y24L peptide is incompatible with formation of ANS-mediated dimers.

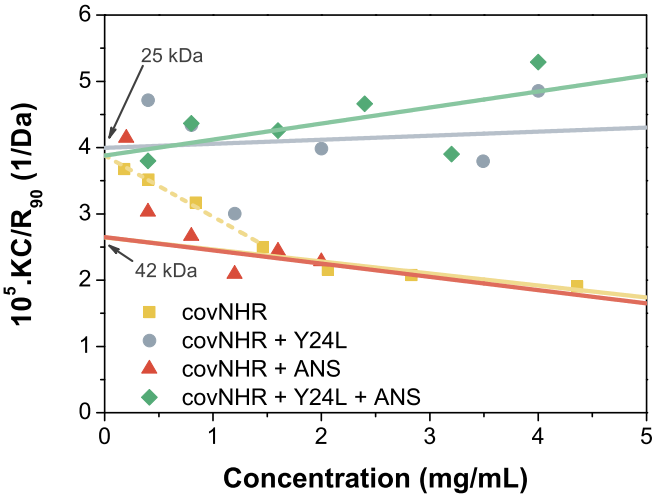

Fig. 5. Debye plots for the static light scattering (SLS) intensity of covNHR with Y24L peptide and ANS in different mixture solutions measured at different protein concentrations. Symbols indicate the experimental results and lines are drawn only for visual purposes.

The ITC titration of covNHR bound to Y24L shows a dramatic change in behavior (Fig. 4C–D). The data comply well with cooperative binding, as suggested by the aforementioned fluorescence titrations. We analyzed the ITC isotherm using a sequential binding model, in which two ANS molecules bind to the HP ($M + A \leftrightarrow MA$; $MA + A \leftrightarrow MA_2$; see Supplementary material). The model reproduces very well the binding isotherms and indicates that two ANS molecules can occupy the HP with positive binding cooperativity.

This dramatic change in the binding mode of ANS to the HP is induced by occupancy of the distant NTP and MP by the Y24L peptide. The thermodynamic parameters of binding derived from this analysis (Table 1) indicate a low affinity binding of a first ANS molecule with slightly positive enthalpy and a second binding event with significantly higher negative enthalpy. The first ANS binding is therefore entropically driven and complies with a mainly hydrophobic interaction of ANS with the HP. In contrast, the second binding event is driven by enthalpy, suggesting a considerable contribution of polar/electrostatic interactions. The cooperativity ratio [42], $\rho = 4 \cdot K_2/K_1 = 5.7 \pm 2.0$, indicates a moderately positive cooperativity. These results clearly show that the HP can hold two ANS molecules establishing energetically favorable communication.

The global enthalpy of ANS binding is much smaller in magnitude than that of binding to the free protein, likely because the bound CHR peptide has already stabilized the protein, removing part of the structural tightening contribution.

Table 1
Thermodynamic parameters of binding of ANS to covNHR protein in free form and bound to the Y24L peptide. Uncertainties in the parameters correspond to standard errors of the fits.

Binding model: $2M + A \leftrightarrow M_2A$		
Protein	K_2 (M^{-2})	ΔH_2 (kJ mol^{-1})
covNHR	$(5.7 \pm 0.3) \times 10^8$	-56.4 ± 1.8
covNHR-Q23I	$(8.4 \pm 0.7) \times 10^8$	-43.7 ± 2.2

Binding model: $M + A \leftrightarrow MA$; $MA + A \leftrightarrow MA_2$				
Protein	K_1 (M^{-1})	ΔH_2 (kJ mol^{-1})	K_2 (M^{-1})	ΔH_2 (kJ mol^{-1})
covNHR+Y24L	$(5.6 \pm 1.1) \times 10^3$	$+0.3 \pm 0.2$	$(8.0 \pm 1.2) \times 10^3$	-36.5 ± 1.5

3.4. Computational modeling and molecular docking

To analyze the ANS binding mode in more detail, we performed a molecular docking simulation study using as template the crystallographic structure of covNHR in complex with C34 (Fig. 6A) (PDB ID: 6R2G) [21]. First, we carried out a blind-docking simulation on the entire protein surface to explore the binding mode of ANS. The top ranked poses in each cluster, regarded as those having the highest binding energy, correspond to binding poses of ANS in the HP. The top ranking conformation for the covNHR-ANS complex (Fig. 6D) evidences

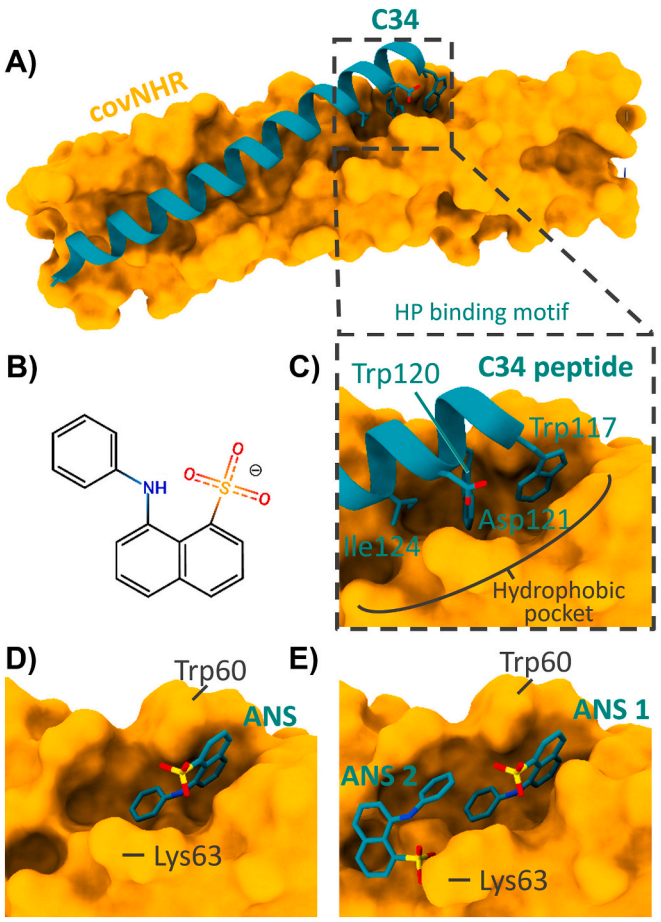

Fig. 6. Structural insight into the ANS binding to the HP pocket of covNHR. A) covNHR in complex with C34 peptide (PDB ID: 6R2G). B) 2D structural representation of ANS molecule colored by atom type. C) Close up view of the HP pocket and the HP binding motif. D) Top scored ANS molecule docked into covNHR showing that it binds to the HP. E) Top scored cluster of ANS molecules sequentially docked into the HP of covNHR in presence of bound Y24L peptide.

that the ANS aromatic rings adopt a similar orientation to that of Trp sidechains of the HP binding motif of C34 (Fig. 6C). This binding pose of ANS within the HP helps to rationalize the results obtained in the previous fluorescence and CD experiments, as peptides owning the HP binding motif displace ANS due to the fact that they share an overlapping binding region (Figs. 1 and 2A and 3).

To inspect the binding mode of ANS within covNHR in complex with Y24L, we conducted a similar docking procedure but this time with the structure of Y24L present in the protein receptor. Because the results obtained in the previous sections reveal that not only one but two molecules of ANS bind cooperatively to covNHR in the presence of Y24L, we carried out a subsequent sequential docking round in order to assess this dual binding mode.

The structure of the complex between covNHR and Y24L was generated as described above but, instead of eliminating the whole C34 peptide, only 10 N-terminal amino acids were removed so that the sequence of Y24L was maintained. After that, as the commercially acquired peptides are *N*-acetylated and C-amidated those residues where added to the respective N- and C-terminal ends of Y24L and the complex structure was energy minimized as described earlier.

We performed a first docking simulation of ANS with the covNHR: Y24L complex structure with the grid box centered on the HP and a box size of 7x7x7 $Å^3$, ensuring a sufficient exploration of the HP to generate favorable interactions. The resulting docking structure was energy minimized as described above. This structure was then used to assess the 2:1 cooperative binding between ANS and covNHR when Y24L peptide is present, by performing a sequential docking experiment with the same parameters as described before. The results of the docking simulations in the presence of Y24L are shown in Fig. 6E. As expected, the first HP-bound ANS molecule (ANS 1) in presence of Y24L adopts a similar conformation to that found in the absence of the peptide. It is interesting to find that two molecules of ANS can be accommodated within the hydrophobic pocket when Y24L peptide is present, in good agreement with the results of the ITC experiments discussed above. Moreover, the spatial orientation of the second bound ANS (ANS 2) is completely upturned relative to ANS 1 and its aromatic groups are less deeply inserted within the HP. These differences are fully consistent with the spectral changes in the near-UV CD bands and with the red-shift in the fluorescence of bound ANS observed in presence of Y24L.

The interactions established between ANS and the residues at the hydrophobic pocket are summarized in Table S2. It is interesting to note that ANS 1 exhibits a higher number of hydrophobic contacts with the surrounding amino acids that constitute the HP. A total of 8 hydrophobic interactions were listed. On the other hand, ANS 2 shows only 3 hydrophobic contacts with the residues at the HP, but it establishes a hydrogen bond with its sulfate group and the amino group of Lys35 (structurally equivalent to Lys63 in gp41 sequence; Table S2). Moreover, both ANS molecules mutually establish a π-π stacking interaction between their aniline moieties. This interaction justifies the observed positive cooperativity of binding between the two ANS molecules.

3.5. Molecular dynamics simulations

To further validate and refine the docking results and assess the stability and dynamic behavior of the covNHR-ANS and covNHR-Y24L-ANS complexes, we carried out 100 ns all-atom explicit-solvent MD simulations using the top scored docking pose of each complex as starting point. Additionally, the structures of free covNHR and the covNHR-Y24L complex were also evaluated with the same MD protocol. The ANS binding poses obtained by docking were stable throughout the entire simulation time without significant differences between the initial and the final ligand poses (Fig. 7).

Fig. 7A shows the time evolution of backbone root mean square deviations (RMSD) of the covNHR protein from each initial structure. All the systems reached equilibrium within the first 20 ns of MD simulation and remain stable throughout the whole simulation time reaching a similar plateau. When comparing the probability distribution function of each system's RMSD (Fig. 7B), small overall reductions in RMSD values can be observed when ANS molecules occupy the HP, suggesting a higher stability of the ANS-bound structures.

Larger differences corroborating these findings can be observed by comparing the evolution of the radius of gyration (Rg), which is a good estimate of the structure compactness (Fig. 7C). Rg values of the covNHR complexes with the different ligands are consistently smaller than the values observed for the free protein during the simulation time. Those differences become more evident when the probability distribution functions of the Rg are compared (Fig. 7D). Binding of Y24L and/or ANS increased progressively the compactness of the system.

Moreover, the root mean square fluctuation (RMSF) values, which are a measurement of the average atomic mobility of the protein in the MD simulations, show an increase in the stability of the protein when it is in presence of ANS and/or Y24L peptide (Fig. 7E). The RMSF mean values decrease with the binding of Y24L peptide or ANS compared to the free protein, and become further decreased for the complex with Y24L and two ANS molecules. This reinforces the idea that the protein complexes are less dynamic than the protein in its free form. The residues at the binding interfaces with the ligands show little fluctuations during the MD simulation time indicating that they form stable interactions with the protein. Interestingly, the main fluctuations correspond to the first and second loop of the protein (together with the N- and C-terminal ends of the protein), which are far from the ligand

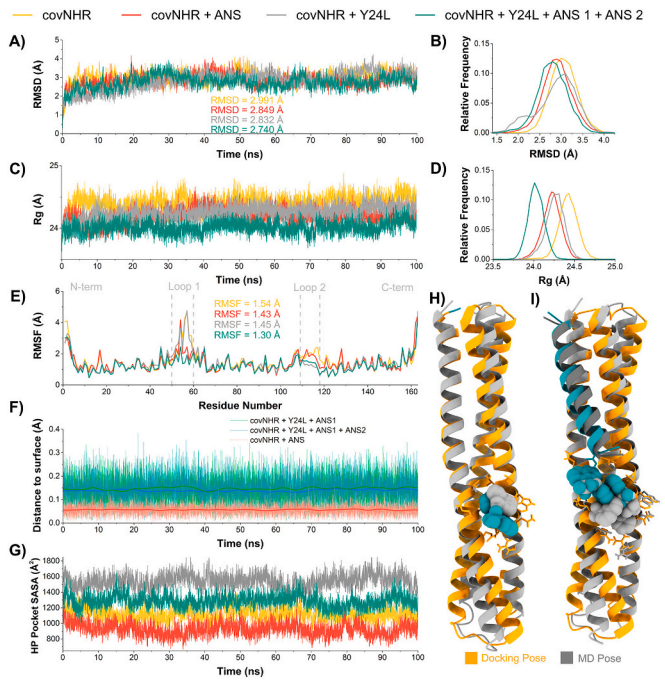

Fig. 7. Molecular dynamics simulations analyses of the four different systems: yellow, free covNHR; red, covNHR in complex with one ANS molecule; gray, covNHR in complex with Y24L; green, covNHR in complex with Y24L and two ANS molecules. A) Evolution of mean backbone root mean square deviation (RMSD) for each simulated system. B) Probability distribution function of RMSD values shown in A). C) Evolution of the radius of gyration (Rg) for each system. D) Probability distribution functions of Rg values shown in C). E) Root mean square fluctuation (RMSF) per residue for each system. F) Evolution of the distance of ANS molecules to the closest point on the surface of covNHR, green and blue lines indicate the distance of ANS 1 and ANS 2 respectively in the covNHR:Y24L; red line indicates the distance of the only ANS molecule present in its complex with covNHR. G) Hydrophobic pocket solvent accessible surface area (SASA) throughout the MD trajectories. The HP area in covNHR was calculated as the sum of SASA of residues: Gln24, Leu27, Gln28, Val31, Ser32, Ile34, Lys35, Gln38, Leu137, Leu140, Thr141, Trp143, Gly144, Ile145, Gln147, Leu148 and Arg151. H, I) Superposed structures between the docking poses and the average MD poses throughout the entire simulation time for H) covNHR and ANS and I) covNHR in complex with both Y24L and two ANS molecules.

interfaces. In addition, the different complexes show reduced fluctuations in these regions, in agreement with an increased stability and a long-range connection between different regions produced by ligand binding, and also related to the observed decrease in Rg values.

The ability of ANS to establish stable interactions is further corroborated by the close contact maintained by the ANS molecules with the protein surface during the whole simulation time (Fig. 7F). ANS molecules bind to the HP and remain in it with little fluctuations during the simulations not dissociating and maintaining a short distance between each ANS molecule and the protein as can be seen in Fig. 7H and I (for the complex covNHR-ANS and covNHR-Y24L-ANS1-ANS2 respectively).

Fig. 7G shows evolution of the HP size throughout the MD trajectories according to the solvent accessible surface area (SASA) of the HP residues in each system calculated removing the ligands. The HP is enlarged in presence of bound Y24L compared to free covNHR, thus facilitating the binding of a second molecule of ANS. Binding of ANS to the HP in either the free protein (red vs yellow in Fig. 7G) or the covNHR-Y24L complex (green vs gray) produces a reduction in SASA of the HP, indicating an induced fit binding of ANS molecules to the receptor regardless of the presence of Y24L peptide. These findings highlight a considerable conformational flexibility of the HP that is modulated by the occupancy of the rest of the hydrophobic groove.

4. Discussion

Finding small-molecule inhibitors targeting the gp41 HP has been a challenging task despite extensive efforts both from scientific community and pharmaceutical companies. One of the reasons is the difficulty to develop a suitable molecular model of gp41 NHR for combined computational and experimental research, as well as for high-throughput screening. We have previously shown that our covNHR proteins are very useful models displaying a functionally relevant HP, as demonstrated by their strong capacity to compete with internal gp41 interactions and to broadly inhibit HIV-1 [20,21,37,38,41]. The results presented here show how this mimetic protein allows a combined experimental-computational study to characterize structurally and energetically two different binding modes of ANS to the HP.

While ANS has been extensively used as a probe for surface exposed hydrophobicity in proteins, it shares several characteristics with other small molecule inhibitors, including aromatic groups and the presence of a negatively charged group. This has been considered a key feature in other inhibitors to interact with the preserved Lys63 side chain at the HP [43]. Also, the docking poses found here imitate the hydrophobic interactions established by the Trp-Trp-Ile pocket-binding motif of CHR. However, we demonstrate that binding of a single ANS molecule to the HP shows an irrelevant affinity because the HP is too large for such a small compound to establish sufficient interactions. This might be applicable to similarly sized compounds that have been tested in the past as potential fusion inhibitors targeting the HP. It has been observed that peptide-based drugs are most effective in inhibiting protein-protein interactions that bury more than 2000 $Å^2$ of accessible surface area, whereas small-molecule compounds usually target smaller interfaces [44]. Therefore, blocking the gp41 6HB formation with small-molecule inhibitors is a great challenge because the NHR-CHR interaction extends along a quite large interface burying more than 3000 $Å^2$ [21] and the binding energy is largely distributed between different pockets on the NHR crevice [37,45]. Nevertheless, the HP continues to be a hotspot in this interaction because its contribution to the overall NHR-CHR binding energy is predominant [37]. Therefore, larger compounds may still constitute good HP binders interfering with 6HB formation provided they fill more completely the HP cavity and establish sufficiently favorable interactions.

We demonstrate here that the HP is conformationally flexible and dynamic and shows allosteric communication with the rest of the NHR is in agreement with our previous work [37]. Therefore, binding at other places of the NHR crevice alters the conformation and interactions at the HP opening it and allowing it to hold two ANS molecules.

The conformational flexibility of the HP reported here might have a functional relevance for the fusion mechanism. Recently, it has been reported that the Trp-rich region of the MPER can also interact with the HP [46]. This binding promiscuity of the HP implies a significant conformational plasticity. However, these MPER-HP interactions should only be transient, as gp41 must progress to its post-fusion conformation for a productive pore formation. The establishment of additional interactions with the CHR along the NHR crevice, possibly involving the MP and NTP pockets, may be key to modulate allosterically the HP conformation, regulate transient interactions, and finally to lock the HP in its high-affinity post-fusion conformation. A more profound understanding of this allosterically regulated process would help to better understand the gp41-driven fusion mechanism and guide the search of more potent inhibitors.

Our results show that the HP can hold up to two ANS molecules in its conformation stabilized by CHR-peptides. The thermodynamic signature of the two sequential binding events together with the docking and MD analysis also helps to understand the mode of interaction. Binding of the first ANS molecule is entropically driven, indicating a mainly hydrophobic interaction. This is consistent with the geometric orientation of the first bound ANS molecule found in our docking study, in which the two aromatic rings insert profoundly into two cavities of the pocket. In

contrast, the binding of the second molecule is enthalpically driven, consistently with a more important contribution of polar interactions. In fact, in the docking pose of the second ANS molecule, its spatial orientation is reversed, so that the sulfate group can interact electrostatically with the side chain of Lys63 (Lys35 in covNHR sequence). This interaction replaces a highly conserved salt bridge between Asp121 and Lys63 in the post-fusion gp41 structure, which plays a critical role in 6HB formation [43]. Moreover, there is a clear stacking between the benzyl rings of the two ANS molecules, which explains the observed binding cooperativity. These results suggest that compounds mimicking this particular molecular geometry and interactions may constitute good leads for new inhibitors targeting the HP. A considerable number of small compounds targeting the HP have been identified or designed previously (recently reviewed in [47]). Many of them were identified by computational screening involving docking analysis or were submitted later to docking protocols to identify the chief interactions. The main features of these compounds with high affinity for the HP have been summarized in several characteristics [48]; namely, an extended hydrophobic scaffold that fills completely the HP [49]; a negatively charged group that can interact electrostatically with Lys63 or Arg68 [50] and/or establish H-bonds with Gln56 or Gln64 [51]; aromatic-ring stacking interactions involving ligand groups and Trp60 in gp41. All these features are perfectly met in the ANS-HP interactions observed in our docking analysis. In fact, the residues lining the HP and the type of interactions involved in ANS binding (Table S2) are largely coincident with those reported in the literature for the most relevant compounds.

The results of our docking and MD studies facilitate potential strategies to identify or design new ANS derivatives with improved binding affinity for the HP. A possible strategy is to reduce the rotational-translational entropy of binding by tethering with an appropriate linker two ANS fragments in a similar orientation to that found in our docking pose. Another possibility is to perform structure similarity virtual screening of compound libraries to identify drug-like compounds with analogous structure to that of the ANS dimer found in our docking poses. Moreover, the discovery of new HP targeting inhibitors may also be facilitated using our covNHR protein by competitive fluorescence-based screening assays, based on the results presented here, to detect HP binding compounds. This potential screening methodology stands out by the ease of using a recombinant protein, which is purified easily and with high yield at a laboratory scale and a widespread fluorescent probe such as ANS.

5. Conclusions

In this study we show that ANS is able to bind specifically to the HP of the gp41 NHR region, a promising target for fusion inhibitors. An experimental structural and thermodynamic characterization combined with computational methods allowed us to discern between two different binding modes of ANS to the HP. The mode of ANS binding is modified allosterically by the occupancy of other NHR pockets by a CHR peptide, demonstrating that the HP shows a marked conformational flexibility. In its stabilized form, the HP can hold two ANS molecules that bind cooperatively, mimicking functionally relevant interactions at the HP.

ANS-based derivative molecules may thus constitute potential drug candidates, providing a valuable class of new lead structures for the design of potent HIV fusion inhibitors. These new structures may be generated upon similarity search within compound libraries or by rational design with the data gathered here. The rational design approach is facilitated by the fact that in this study we exposed a possible way of interaction between this small-molecule and its protein target, which may guide the designing step towards more potent inhibitors. Discovery of the novel scaffolds and binding mechanism suggests avenues for extending the interaction surface and improving the potency of HP-targeting inhibitors.

CRediT authorship contribution statement

Mario Cano-Muñoz: Conceptualization, Investigation, Methodology, Software, Data curation; Formal analysis; Writing - original draft. **Samuel Jurado**: Investigation. **Bertrand Morel**: Methodology, Supervision. **Francisco Conejero-Lara**: Conceptualization, Data curation, Formal analysis, Funding acquisition, Project administration, Writing - review & editing.

Declaration of competing interest

Authors declare there is no conflict of interest.

Acknowledgements

We thank Dr. Angel Pey for his fruitful comments and discussion. This research was funded by the Spanish State Research Agency, SRA/10.13039/501100011033 (grants BIO2016-76640-R and PID2019.107515RB.C21), co-funded by ERDF/ESF, "A way to make Europe"/"Investing in your future". The results shown are included as part of MCM doctoral thesis.

Appendix A. Supplementary data

Supplementary data to this article can be found online at https://doi.org/10.1016/j.ijbiomac.2021.09.198.

References

[1] D.C. Chan, P.S. Kim, HIV entry and its inhibition, Cell 93 (1998) 681–684, https://doi.org/10.1016/s0092-8674(00)81430-0.
[2] J.M. White, S.E. Delos, M. Brecher, K. Schornberg, Structures and mechanisms of viral membrane fusion proteins: multiple variations on a common theme, Crit. Rev. Biochem. Mol. 43 (2008) 189–219, https://doi.org/10.1080/10409230802058320.
[3] A.C. Walls, Y.J. Park, M.A. Tortorici, A. Wall, A.T. McGuire, D. Veesler, Structure, Function, and antigenicity of the SARS-CoV-2 spike glycoprotein, Cell 181 (2020) 281–292 e286, https://doi.org/10.1016/j.cell.2020.02.058.
[4] UNAIDS, UNAIDS Data 2020, 2020. http://www.unaids.org/sites/default/files/media_asset/2020_aids-data-book_en.pdf. (Accessed 18 April 2021).
[5] P. Iyidogan, K.S. Anderson, Current perspectives on HIV-1 antiretroviral drug resistance, VirusBasel 6 (2014) 4095–4139, https://doi.org/10.3390/v6104095.
[6] B.F. Silva, G.M.L. Peixoto, S.R. da Luz, S.M.F. de Moraes, S.B. Peres, Adverse effects of chronic treatment with the Main subclasses of highly active antiretroviral therapy: a systematic review, HIV Med. 20 (2019) 429–438, https://doi.org/10.1111/hiv.12733.
[7] A.B. Ward, I.A. Wilson, The HIV-1 envelope glycoprotein structure: nailing down a moving target, Immunol. Rev. 275 (2017) 21–32, https://doi.org/10.1111/imr.12507.
[8] W. Weissenhorn, A. Dessen, S.C. Harrison, J.J. Skehel, D.C. Wiley, Atomic structure of the ectodomain from HIV-1 gp41, Nature 387 (1997) 426–430, https://doi.org/10.1038/387426a0.
[9] D.C. Chan, D. Fass, J.M. Berger, P.S. Kim, Core structure of gp41 from the HIV envelope glycoprotein, Cell 89 (1997) 263–273, https://doi.org/10.1016/s0092-8674(00)80205-6.
[10] H.A. Yi, B.C. Fochtman, R.C. Rizzo, A. Jacobs, Inhibition of HIV entry by targeting the envelope transmembrane subunit gp41, Curr. HIV Res. 14 (2016) 283–294, https://doi.org/10.2174/1570162x14999160224103908.
[11] J.M. Kilby, S. Hopkins, T.M. Venetta, B. DiMassimo, G.A. Cloud, J.Y. Lee, L. Alldredge, E. Hunter, D. Lambert, D. Bolognesi, T. Mathews, M.R. Johnson, M. A. Nowak, G.M. Shaw, M.S. Saag, Potent suppression of HIV-1 replication in humans by T-20, a peptide inhibitor of gp41-mediated virus entry, Nat. Med. 4 (1998) 1302–1307, https://doi.org/10.1038/3293.
[12] L. Cai, S. Jiang, Development of peptide and small-molecule HIV-1 fusion inhibitors that target gp41, ChemMedChem 5 (2010) 1813–1824, https://doi.org/10.1002/cmdc.201000289.
[13] S.B. Jiang, H. Lu, S.W. Liu, Q. Zhao, Y.X. He, A.K. Debnath, N-substituted pyrrole derivatives as novel human immunodeficiency virus type 1 entry inhibitors that interfere with the gp41 six-helix bundle formation and block virus fusion, Antimicrob. Agents Chemother. 48 (2004) 4349–4359, https://doi.org/10.1128/aac.48.11.4349-4359.2004.
[14] K. Lu, M.R. Asyifah, F. Shao, D. Zhang, Development of HIV-1 fusion inhibitors targeting gp41, Curr. Med. Chem. 21 (2014) 1976–1996, https://doi.org/10.2174/0929867321666131218094559.
[15] L. Lu, F. Yu, L. Cai, A.K. Debnath, S. Jiang, Development of small-molecule HIV entry inhibitors specifically targeting gp120 or gp41, Curr. Top. Med. Chem. 16 (2016) 1074–1090.

[16] G.Y. Zhou, D. Wu, B. Snyder, R.G. Ptak, H. Kaur, M. Gochin, Development of indole compounds as small molecule fusion inhibitors targeting HIV-1 Glycoprotein-41, J. Med. Chem. 54 (2011) 7220–7231, https://doi.org/10.1021/jm200791z.
[17] D.M. Eckert, P.S. Kim, Design of potent inhibitors of HIV-1 entry from the gp41 N-peptide region, Proc. Natl. Acad. Sci. U. S. A. 98 (2001) 11187–11192, https://doi.org/10.1073/pnas.201392898.
[18] M.J. Root, M.S. Kay, P.S. Kim, Protein design of an HIV-1 entry inhibitor, Science 291 (2001) 884–888, https://doi.org/10.1126/science.1057453.
[19] F. Yu, L. Lu, L.Y. Du, X.J. Zhu, A.K. Debnath, S.B. Jiang, Approaches for identification of HIV-1 entry inhibitors targeting gp41 pocket, VirusBasel 5 (2013) 127–149, https://doi.org/10.3390/v5010127.
[20] S. Crespillo, A. Camara-Artigas, S. Casares, B. Morel, E.S. Cobos, P.L. Mateo, N. Mouz, C.E. Martin, M.G. Roger, R. El Habib, B. Su, C. Moog, F. Conejero-Lara, Single-chain protein mimetics of the N-terminal heptad-repeat region of gp41 with potential as anti-HIV-1 drugs, Proc. Natl. Acad. Sci. U. S. A. 111 (2014) 18207–18212, https://doi.org/10.1073/pnas.1413592112.
[21] S. Jurado, M. Cano-Munoz, B. Morel, S. Standoli, E. Santarossa, C. Moog, S. Schmidt, G. Laumond, A. Camara-Artigas, F. Conejero-Lara, Structural and thermodynamic analysis of HIV-1 fusion inhibition using small gp41 mimetic proteins, J. Mol. Biol. 431 (2019) 3091–3106, https://doi.org/10.1016/j.jmb.2019.06.022.
[22] F. Manssour-Triedo, S. Crespillo, B. Morel, S. Casares, P.L. Mateo, F. Notka, M. G. Roger, N. Mouz, R. El-Habib, F. Conejero-Lara, Molecular and physicochemical factors governing solubility of the HIV gp41 ectodomain, Biophys. J. 111 (2016) 700–709, https://doi.org/10.1016/j.bpj.2016.07.022.
[23] A. Hawe, M. Sutter, W. Jiskoot, Extrinsic fluorescent dyes as tools for protein characterization, Pharm. Res. 25 (2008) 1487–1499, https://doi.org/10.1007/s11095-007-9516-9.
[24] C.A. Lipinski, F. Lombardo, B.W. Dominy, P.J. Feeney, Experimental and computational approaches to estimate solubility and permeability in drug discovery and development settings, Adv. Drug Deliv. Rev. 23 (1997) 3–25, https://doi.org/10.1016/s0169-409x(96)00423-1.
[25] M.R. Wilkins, E. Gasteiger, A. Bairoch, J.-C. Sanchez, K.L. Williams, R.D. Appel, D. F. Hochstrasser, Protein identification and analysis tools in the ExPASy server, in: Methods in Molecular Biology; 2-D proteome analysis protocols, 1999, pp. 531–552.
[26] R.F. Latypov, D. Liu, K. Gunasekaran, T.S. Harvey, V.I. Razinkov, A.A. Raibekas, Structural and thermodynamic effects of ANS binding to human interleukin-1 receptor antagonist, Protein Sci. 17 (2008) 652–663, https://doi.org/10.1110/ps.073332408.
[27] A.V. Fonin, A.I. Sulatskaya, I.M. Kuznetsova, K.K. Turoverov, Fluorescence of dyes in solutions with high absorbanceInner Filter Effect Correction, PLoS One 9 (2014), e103878, https://doi.org/10.1371/journal.pone.0103878.
[28] E. Krieger, G. Vriend, YASARA view-molecular graphics for all devices-from smartphones to workstations, Bioinformatics 30 (2014) 2981–2982, https://doi.org/10.1093/bioinformatics/btu426.
[29] E. Krieger, G. Koraimann, G. Vriend, Increasing the precision of comparative models with YASARA NOVA - a self-parameterizing force field, Proteins 47 (2002) 393–402, https://doi.org/10.1002/prot.10104.
[30] U. Essmann, L. Perera, M.L. Berkowitz, T. Darden, H. Lee, L.G. Pedersen, A smooth particle mesh ewald method, J. Chem. Phys. 103 (1995) 8577–8593, https://doi.org/10.1063/1.470117.
[31] G.M. Morris, R. Huey, W. Lindstrom, M.F. Sanner, R.K. Belew, D.S. Goodsell, A. J. Olson, AutoDock4 and AutoDockTools4: automated docking with selective receptor flexibility, J. Comput. Chem. 30 (2009) 2785–2791, https://doi.org/10.1002/jcc.21256.
[32] Y. Duan, C. Wu, S. Chowdhury, M.C. Lee, G.M. Xiong, W. Zhang, R. Yang, P. Cieplak, R. Luo, T. Lee, J. Caldwell, J.M. Wang, P. Kollman, A point-charge force field for molecular mechanics simulations of proteins based on condensed-phase quantum mechanical calculations, J. Comput. Chem. 24 (2003) 1999–2012, https://doi.org/10.1002/jcc.10349.
[33] M. Medina-O'Donnell, F. Rivas, F.J. Reyes-Zurita, M. Cano-Munoz, A. Martinez, J. A. Lupianez, A. Parra, Oleanolic acid derivatives as potential inhibitors of HIV-1 protease, J. Nat. Prod. 82 (2019) 2886–2896, https://doi.org/10.1021/acs.jnatprod.9b00649.
[34] G.M. Morris, D.S. Goodsell, R.S. Halliday, R. Huey, W.E. Hart, R.K. Belew, A. J. Olson, Automated docking using a lamarckian genetic algorithm and an empirical binding free energy function, J. Comput. Chem. 19 (1998) 1639–1662, https://doi.org/10.1002/(sici)1096-987x(19981115)19:14<1639::aid-jcc10>3.0.co;2-b.
[35] E. Krieger, J.E. Nielsen, C.A.E.M. Spronk, G. Vriend, Fast empirical pK(a) prediction by ewald summation, J. Mol. Graph. 25 (2006) 481–486, https://doi.org/10.1016/j.jmgm.2006.02.009.
[36] V. Hornak, R. Abel, A. Okur, B. Strockbine, A. Roitberg, C. Simmerling, Comparison of multiple amber force fields and development of improved protein backbone parameters, Proteins 65 (2006) 712–725, https://doi.org/10.1002/prot.21123.
[37] S. Jurado, M. Cano-Munoz, D. Polo-Megias, F. Conejero-Lara, B. Morel, Thermodynamic dissection of the interface between HIV-1 gp41 heptad repeats reveals cooperative interactions and allosteric effects, Arch. Biochem. Biophys. 688 (2020), 108401, https://doi.org/10.1016/j.abb.2020.108401.
[38] S. Jurado, C. Moog, M. Cano-Munoz, S. Schmidt, G. Laumond, V. Ruocco, S. Standoli, D. Polo-Megias, F. Conejero-Lara, B. Morel, Probing vulnerability of the gp41 C-terminal heptad repeat as target for miniprotein HIV inhibitors, J. Mol. Biol. 432 (2020) 5577–5592, https://doi.org/10.1016/j.jmb.2020.08.010.
[39] S.B. Jasim, Z. Li, E.E. Guest, J.D. Hirst, DichroCalc: improvements in computing protein circular dichroism spectroscopy in the near-ultraviolet, J. Mol. Biol. 430 (2018) 2196–2202, https://doi.org/10.1016/j.jmb.2017.12.009.
[40] E. Klimtchuk, S. Venyaminov, E. Kurian, W. Wessels, W. Kirk, F.G. Prendergast, Photophysics of ANS. I., Protein-ANS complexes: intestinal fatty acid binding protein and single-trp mutants, Biophys. Chem. 125 (2007) 1–12, https://doi.org/10.1016/j.bpc.2006.07.016.
[41] M. Cano-Munoz, S. Cesaro, B. Morel, J. Lucas, C. Moog, F. Conejero-Lara, Extremely thermostabilizing Core mutations in coiled-coil mimetic proteins of HIV-1 gp41 produce diverse effects on target binding but do not affect their inhibitory activity, Biomolecules 11 (2021) 566, https://doi.org/10.3390/biom11040566.
[42] E. Freire, A. Schön, A. Velazquez-Campoy, Isothermal titration calorimetry: general formalism using binding polynomials, Methods Enzymol. 455 (2009) 127–155, https://doi.org/10.1016/s0076-6879(08)04205-5.
[43] Y. He, S. Liu, W. Jing, H. Lu, D. Cai, D.J. Chin, A.K. Debnath, F. Kirchhoff, S. Jiang, Conserved residue Lys574 in the cavity of HIV-1 Gp41 coiled-coil domain is critical for six-helix bundle stability and virus Entry*, J. Biol. Chem. 282 (2007) 25631–25639, https://doi.org/10.1074/jbc.M703781200.
[44] X. Ran, J.E. Gestwicki, Inhibitors of protein-protein interactions (PPIs): an analysis of scaffold choices and buried surface area, Curr. Opin. Chem. Biol. 44 (2018) 75–86, https://doi.org/10.1016/j.cbpa.2018.06.004.
[45] L.M. Johnson, W.S. Horne, S.H. Gellman, Broad distribution of energetically important contacts across an extended protein interface, J. Am. Chem. Soc. 133 (2011) 10038–10041, https://doi.org/10.1021/ja203358t.
[46] Y. Zhu, X. Ding, D. Yu, H. Chong, Y. He, The tryptophan-rich motif of HIV-1 gp41 can interact with the N-terminal deep pocket site: new insights into the structure and function of gp41 and its inhibitors, J. Virol. 94 (2019), https://doi.org/10.1128/jvi.01358-19 e01358-01319.
[47] T.M. Rad, L. Saghaie, A. Fassihi, HIV-1 entry inhibitors: a review of experimental and computational studies, Chem. Biodivers. 15 (2018), e1800159, https://doi.org/10.1002/cbdv.201800159.
[48] S. Sepehri, L. Saghaie, A. Fassihi, Anti-HIV-1 activity prediction of novel Gp41 inhibitors using structure-based virtual screening and molecular dynamics simulation, Mol. Inf. 36 (2017) 1600060, https://doi.org/10.1002/minf.201600060.
[49] R. Munnaluri, S.K. Sivan, V. Manga, Molecular docking and MM/GBSA integrated protocol for designing small molecule inhibitors against HIV-1 gp41, Med. Chem. Res. 24 (2015) 829–841, https://doi.org/10.1007/s00044-014-1185-8.
[50] S.B. Jiang, A.K. Debnath, A salt bridge between an N-terminal coiled coil of gp41 and an antiviral agent targeted to the gp41 cove is important for anti-HIV-1 activity, Biochem. Biophys. Res. Commun. 270 (2000) 153–157, https://doi.org/10.1006/bbrc.2000.2411.
[51] S. Sepehri, S. Soleymani, R. Zabihollahi, M.R. Aghasadeghi, M. Sadat, L. Saghaie, A. Fassihi, Synthesis, biological evaluation, and molecular docking studies of novel 4–4-arylpyridin-1(4H)-yl benzoic acid derivatives as anti-HIV-1 agents, Chem. Biodivers. 14 (2017), e1700295, https://doi.org/10.1002/cbdv.201700295.